Solitary wave billiards

Item Type	article
Authors	Cuevas-Maraver, Jesús;Kevrekidis, Panayotis G.;Zhang, Hongkun
DOI	10.48550/arXiv.2203.09489
Rights	UMass Amherst Open Access Policy
Download date	2025-08-15 13:25:27
Link to Item	https://hdl.handle.net/20.500.14394/34391

Solitary wave billiards

Jesús Cuevas-Maraver

Grupo de Física No Lineal, Departamento de Física Aplicada I,
Universidad de Sevilla. Escuela Politécnica Superior, C/ Virgen de Africa, 7, 41011-Sevilla, Spain and
Instituto de Matemáticas de la Universidad de Sevilla (IMUS). Edificio Celestino Mutis. Avda. Reina Mercedes s/n,
41012-Sevilla, Spain, Avda Reina Mercedes s/n, 41012 Sevilla, Spain

Panayotis G. Kevrekidis and Hongkun Zhang

Department of Mathematics and Statistics, University of Massachusetts, Amherst, Massachusetts 01003-4515, USA

In the present work we introduce the concept of solitary wave billiards. I.e., instead of a point particle, we consider a solitary wave in an enclosed region and explore its collision with the boundaries and the resulting trajectories in cases which for particle billiards are known to be integrable and for cases that are known to be chaotic. A principal conclusion is that solitary wave billiards are generically found to be chaotic even in cases where the classical particle billiards are integrable. However, the degree of resulting chaoticity depends on the particle speed and on the properties of the potential. Furthermore, the nature of the scattering of the deformable solitary wave particle is elucidated on the basis of a negative Goos-Hänchen effect which, in addition to a trajectory shift, also results in an effective shrinkage of the billiard domain.

I. INTRODUCTION

In recent years, the study of solitary waves has been a topic of widespread appeal in a broad range of fields. For instance, relevant coherent structures arise in the exploration of electrical field dynamics within optical fibers [1, 2], as well as in the study of nonlinear effects in plasmas [3]. They emerge in atomic clouds of Bose-Einstein condensates (BECs) [4, 5], as well as in so-called rogue waves in the ocean [6]. Of central role within most of the above studies and fields has been the envelope wave model of the nonlinear Schrödinger equation [7–10], which can be used to describe the electric field of light, the wavefunction of BEC atoms, or the water wave elevation. Indeed, the resulting nonlinearity may stem from different sources, such as e.g., the so-called Kerr effect in optics [1, 2] or an effective mean-field nonlinearity due to contact interactions between bosons [4, 5], yet its impact is similar across fields in producing robust solitary waves of either bright [2, 10], dark [11] or rogue [6] form.

On the other hand, the notion of billiards is one that has attracted significant attention both at the classical, as well as at the quantum side. Here, a point particle is reflected within a (typically) enclosed 2D domain Q (of different possible shapes) [12, 13] (see also [14] for an extensive set of references). The particle moves freely aside from its interaction with the boundary ∂Q, by elastic reflections without loss of speed. Depending on the nature of the billiard (e.g., square or circular or instead an elliptical stadium [15, 16] or a square with an enclosed circle [12, 17]), the outcome of the reflections could be a closed trajectory associated with integrable motion, or an ergodic trajectory associated with a chaotic billiard.

While the above aspects involve classical billiards, we do note in passing the consideration of quantum billiards. The quantum mechanical billiard is given by the linear Schrödinger equation typically with Dirichlet boundary condition. It describes a wave function associated with a probability density $|\psi|^2$ within the domain while the wall features an infinite potential wall. A relevant summary of some of the activity in the context of experiments (and theory) in the theme of microwave billiards and the connections to quantum chaos can be found in [18], where a number of references to this theme are summarized. The dynamics of quantum billiard are determined by the Hamiltonian equations of motion on the domain Q. The wave function ψ of a single quantum particle with unit mass obeys the Schrödinger equation

$$i\frac{\partial \psi}{\partial t} = -\nabla^2 \psi + V(\mathbf{r})\psi, \qquad \mathbf{r} = (x,y) \in int(Q) \tag{1}$$

with, e.g., Dirichlet boundary conditions $\psi(x,y) = 0$, for $(x,y) \in \partial Q$. Usually one can assume in such a setting that $V(x,y) = 0$ for $(x,y) \in int(Q)$, and $V(x,y) = \infty$, for $(x,y) \in \partial Q$. Most research has been concentrated, for such quantum billiards, on the search for quantum chaos. Even though it was proved that if classical billiard is ergodic, then the corresponding quantum billiard is quantum ergodic, so-called quantum "scars" are observed in most cases, which demonstrate that quantum billiards are more complicated. The Bunimovich stadium [15, 16] has recently become a very popular quantum billiard model, while the study of quantum chaos in different billiards is generally a topic that is gaining considerable traction [19–21].

A less studied billiard is the "soft" version, where the boundary of the billiard table Q is defined by a finite potential wall V, with $V(x,y) = 0$, for $(x,y) \in int(Q)$, and $V(x,y) \in (0,\infty)$ for $(x,y) \in \partial Q$. In such a setting, for a Sinai (dispersing) billiard [12, 17], the existence of a stable island around a periodic orbit which is tangent to the billiard's wall (or near the corner) was found numerically in [22]; see also [23, 24] for other examples of such soft billiards.

In the present work our aim is to introduce a notion that in a sense interweaves the above concepts while paving a new avenue involving the interplay of nonlinearity, billiards and possibly quantum mechanics (but also perhaps more concretely in our

examples below, nonlinear optics) in the form of *solitary wave billiards*. In particular, the connections are quite natural: solitary waves are typically thought of as effective particles (indeed, hence the name) [2, 7–11]. Therefore, it is natural to examine these effective particles in a billiard setting. At the same time, nonlinear Schrödinger equation models appear in a natural sense to generalize the concept of linear quantum billiards in the presence of different types of nonlinearity, stemming from nonlinear optics [2], plasmas [3] or atomic BECs [11]. In that light too, it is useful to adapt some of the ideas of linear quantum billiards to such more complex cases where the localized wavefunction is held together because of the interplay of nonlinearity and dispersion while slowly losing some of its initial kinetic energy through the (potential) interactions with the wall. In that vein, the notion of a soft billiard is a natural one as the solitary wave interacts with a finite potential wall. However, the interaction may be inelastic even in the context of an infinite potential due to the non-integrability of the PDE model. The latter is the typical scenario in the associated $2 + 1$-dimensional spatio-temporal models. It is worthwhile to mention here that the idea of billiards in settings such as BECs has not only been theoretically explored [25, 26], but also experimentally realized in the form of an optically induced confinement potential (i.e., billiard) for the ultracold atoms [27].

However, introducing such solitary wave billiard ideas requires some extra care. One needs to avoid the hurdle of collapse (arising, e.g., in $2 + 1$-dimensional cubic nonlinearity models [10]). Instead one needs to consider a nonlinearity that allows for a robust $2 + 1$-dimensional standing wave; here the saturable nonlinearity of relevance to photorefractive crystals is thus selected [28] as a physically relevant example. Then, the solitary wave is boosted using a Galilean transformation and the billiard dynamics is accordingly initiated. In what follows, we discuss our numerical observations and an emerging qualitative understanding of the relevant phenomenology. We also note in passing that, to our knowledge, no Hamiltonian variant of this type has been considered in the literature. A dissipative (but limited parametrically and lacking the generic ability to produce traveling waves as compared, e.g., with the Galilean transformation of our example) analogue of such concepts has been presented in [32]. Our presentation of the results is structured as follows. In section II, we present the mathematical setup of the problem. In section III, we discuss the numerical observations and their comparison to the point billiard model. Finally, in section IV, we summarize our findings and present some conclusions and directions for future study.

II. MATHEMATICAL SETUP

A. Solition wave billiard

We start from a two-dimensional nonlinear Schrödinger (NLS) equation with (saturable) photorefractive nonlinearity [28],

$$i\psi_t = \mathcal{L}(\psi), \quad \mathcal{L}(\psi) = -\nabla^2\psi + V(\mathbf{r})\psi - \frac{2|\psi|^2}{1 + |\psi|^2}\psi, \quad \mathbf{r} = (x, y) \in Q \tag{2}$$

with $V(\mathbf{r})$ being the potential where the relevant geometry of the billiard will be introduced on Q, and $\nabla^2\psi = \psi_{xx} + \psi_{yy}$. Here, $\psi(\mathbf{r}, t)$ represents the envelope of the electromagnetic field for the optical problem of interest, with the density $\rho = |\psi|^2$ corresponding to the light intensity. While the particular nonlinearity is less directly relevant to atomic BECs, one can envision other nonlinearities there (e.g., competing ones as in the recently budding field of quantum droplets [29]) that can lead to a similar phenomenology. In the latter case $\psi(\mathbf{r}, t)$ plays the role of the condensate wavefunction, while $|\psi|^2$ represents the atomic density. In the optical setting, the potential $V(\mathbf{r})$ stems from the refractive index profile [30], while in BECs, the ability to "paint" arbitrary (and, hence, also billiard) potentials has been demonstrated [31].

The above dynamical equation can be derived from a Hamiltonian formulation as:

$$i\psi_t = \frac{\delta H[\psi]}{\delta\psi^*} \tag{3}$$

where $H[\psi]$ is the (conserved during the dynamics) Hamiltonian functional:

$$H[\psi] = \int_{\mathbf{r}\in Q} \left[|\nabla\psi|^2 + (V(\mathbf{r}) - 2)|\psi|^2 + 2\log(1 + |\psi|^2)\right]\,\mathrm{d}\mathbf{r}. \tag{4}$$

The initial condition for our dynamical simulations will be a stationary solitary wave set into motion by means of a Galilean boost. This is a desirable feature of the present model in comparison with, e.g., the dissipative variant of [32] as the traveling waves herein can be generically achieved and with arbitrarily selected speeds due to the Galilean invariance. The stationary state is found by introducing the ansatz

$$\psi(x, y; t) = \exp(i\omega t)\phi_\omega(x, y) \tag{5}$$

into Eq. (2). It follows that ϕ_ω, if it exists, is a nonlinear eigenfunction of $\mathcal{F}$:

$$-\omega\phi_\omega = \mathcal{F}(\phi_\omega) = -\nabla^2\phi_\omega + V(x, y)\phi_\omega - \frac{2|\phi_\omega|^2}{1 + |\phi_\omega|^2}\phi_\omega.$$

Once this stationary wave is found, we fix ω, and the initial condition of the simulation is attained from the Galilean boost of the stationary structure centered at $(x, y) = (0, 0)$.

$$\psi_0(x, y) \equiv \psi(x, y; 0) = \phi_\omega(x, y) \exp(i(k_x x + k_y y)) = \phi_\omega(x, y) \exp(ik(x \cos\theta + y \sin\theta)) \tag{6}$$

leading to a wave moving with an initial velocity $v_0 = 2|\mathbf{k}|$ that forms an angle θ with the x-axis, and $\mathbf{k} = (k_x, k_y) = |\mathbf{k}|(\cos\theta, \sin\theta)$. Consequently, the energy imparted to the moving coherent structure (in comparison to its stationary state) is given by

$$\Delta E \equiv E[\psi_0(x, y)] - E[\phi_\omega(x, y)] = \int \mathrm{d}^2 r \left[|\nabla \psi_0|^2 - |\nabla \phi_\omega|^2 \right] = N|\mathbf{k}|^2 \tag{7}$$

and is naturally associated with the excess kinetic energy, with N being the squared L^2 norm or the mass, as it is often referred to, of the stationary state

$$N = \int_Q |\phi_\omega|^2 \, d\mathbf{r}. \tag{8}$$

Assigning $N \equiv m$ to an effective mass, we can express this excess energy as:

$$\Delta E = 2m|\mathbf{k}|^2 = \frac{1}{2} m v_0^2 \tag{9}$$

If we suppose that the solitary is moving in a vanishing potential landscape, it can be considered as a quasi-particle that freely moves with a initial kinetic energy equal to ΔE, and this quasi-particle can be interpreted as possessing an effective mass m.

Note that at each time $t \geq 0$, the solitonic wave function $\psi(x, y, t)$, which starts from $\psi_0(x, y)$, defines a reference probability measure $\nu(t)$ on the σ-algebra of the billiard table Q, with density function

$$\rho(\mathbf{r}, t) = \frac{|\psi(\mathbf{r}, t)|^2}{\int |\psi(\mathbf{r}, t)|^2 \, d\mathbf{r}}$$

Using this reference measure, we can investigate some physical quantities (given by expected position, variance, and more general moments) of the solitary wave billiard. To study this billiard $\psi(x, y, t)$, we first consider its center of mass trajectory $\gamma(t)$, which describes the expected position of the coherent structure. More precisely, the expected position of the localized pattern with respect to the reference measure ν is defined as

$$\gamma(t) := \mathbb{E}_{\nu(t)}(\mathbf{r}) = \int_Q (x, y)\rho(\mathbf{r}, t) \, d\mathbf{r}$$

Since $\mathbf{r} = (x, y)$, we also can wrote $\gamma(t) = (X(t), Y(t))$ with

$$X(t) = \mathbb{E}_\nu(x) = \int x \, d\nu, \quad Y(t) = \mathbb{E}_\nu(y) = \int y \, d\nu,$$

as the expected x and y position of the solitary wave, respectively. Note that $(X(t), Y(t))$ can also be interpreted as the center position of the relevant pattern. In the following sections, we will mainly focus on the study of $\mathbf{r}(t) = (X(t), Y(t))$ numerically.

To assess how well the expected position $\bar{\mathbf{r}}(t)$ of the solitary wave within the billiard describes its motion, we also calculate the variance of $\mathbf{r}$ with respect to the reference measure $\nu(t)$:

$$\mathrm{Var}_{\nu(t)}(\mathbf{r}) := \mathbb{E}_{\nu(t)}(\|\mathbf{r} - \gamma(t)\|^2) = \int_{\mathbf{r} \in Q} \left((x - X(t))^2 + (y - Y(t))^2) \right) \rho(\mathbf{r}, t) d\mathbf{r}$$

This quantity characterizes the width of our solitary wave. For narrower solitary waves, it is enough to study the center of mass orbit $\gamma(t)$, corresponding to the solitonic wavefunction $\psi(x, y, t)$.

III. NUMERICAL RESULTS

A. Numerical simulation setup of the dynamical orbit within the solitary wave billiard

In our simulation, to simplify the calculations, we first locate the solitary wave at the point of maximal probability density $\rho(\mathbf{r}, t)$, which is denoted as $\tilde{\gamma}(t) = (\tilde{x}(t), \tilde{y}(t))$ such that for any $t \geq 0$,

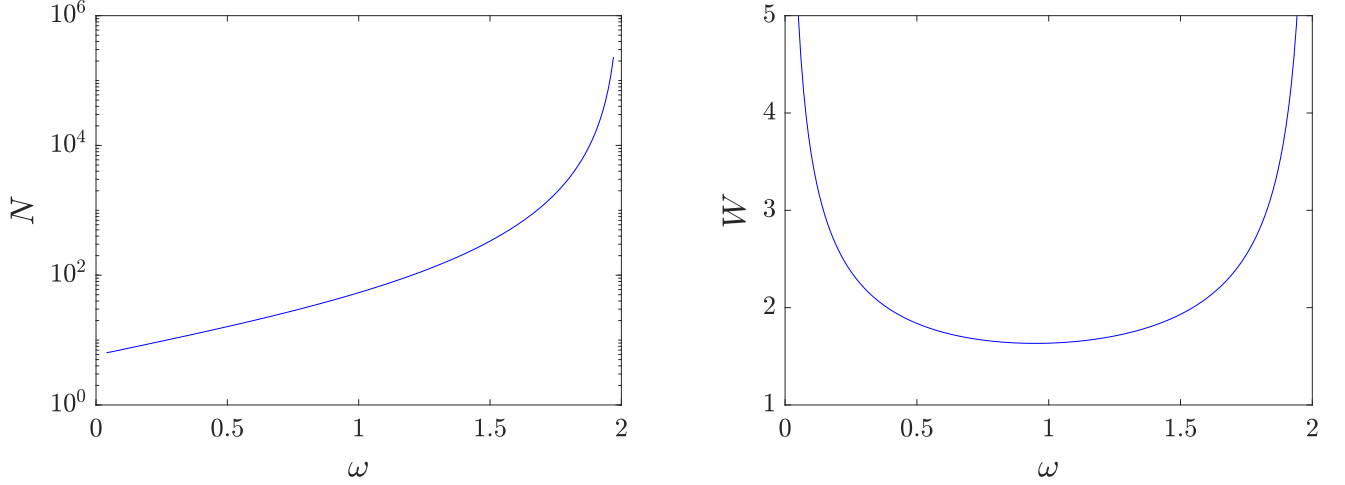$$\rho(\tilde{\gamma}(t)) = \max_{\mathbf{r} \in Q} \rho(\mathbf{r}, t)$$

FIG. 1. Dependence of the norm and the width of the solitary wave with respect to its frequency for the relevant family of solutions.

Our computations suggest that the curve $\rho(\tilde{\gamma}(t))$ is well-defined, i.e. for each t, there is only one (principal, i.e., above a selected cutoff) local maximum for the density function. We subsequently consider a window of size $2\delta \times 2\delta$ centered on $\tilde{\gamma}(t)$, and denote it as $U_\delta(t) \subset Q$; this is suitably adjusted when the wave is in the vicinity of the boundary. In our simulation, we select $\delta = 4$.

The conditional probability measure $\hat{\nu} := \nu|_{U_\delta(t)}$ with density function $\hat{\rho}$ can be calculated as

$$\hat{\rho}(\mathbf{r}, t) = \frac{|\psi(\mathbf{r}, t)|^2 \, \mathbf{I}_{U_\delta(t)}}{\int_{U_\delta(t)} |\psi(\mathbf{r}, t)|^2 \, d\mathbf{r}}$$

Moreover, the simulated expected position of the solitary wave within the billiard with respect to the conditional measure $\hat{\nu}$ can be calculated as

$$(\hat{X}(t), \hat{Y}(t)) := \mathbb{E}_{\hat{\nu}(t)}(\mathbf{r}) = \int_Q (x, y)\hat{\rho}(\mathbf{r}, t) \, d\mathbf{r}.$$

This also provides a smoother and more accurate evaluation of the center of mass, in comparison to the argmax over the numerical grid. Furthermore, the variance associated with the solitary wave position is given by:

$$W(t) := \int_{\mathbf{r} \in Q} \left((x - \hat{X}(t))^2 + (y - \hat{Y}(t))^2) \right) \hat{\rho}(\mathbf{r}, t) d\mathbf{r}$$

In Fig. 1, one can see that the narrowest solitary wave is found for $\omega = 0.95$, and that the associated frequency lies in $\omega \in (0, 2)$ interval, with the lower limit corresponding to the bifurcation of the solitary from the linear modes (continuous spectrum) band, while the upper limit, reflects a divergence of its mass.

In our study, we mainly consider waves with frequency $\omega = 0.5$. In the case examples that follow, we will either consider infinite potentials (implemented via Dirichlet boundary conditions) or finite potentials that are strictly higher than the above-mentioned kinetic energy of the solitary wave, so as to ensure a genuine billiard situation in which the coherent structure will be reflected from the potential walls.

B. Goos-Hänchen shifts of reflection upon potential walls

Before delving into the systematics of the solitary wave trajectories within the entire billiard, we briefly highlight a key feature of the billiard reflection of the wave upon collision with the potential walls, for the case when the potential V is finite at the boundary of Q.

When describing total reflection of a solitary wave in such a billiard potential setting, we need to identify expressions for the phase shift that occurs for each such event between the incident and reflected waves as a function of angle of incidence. This phase shift is attributed to the fact that some energy is stored at the potential wall before returning to the reflected wave.
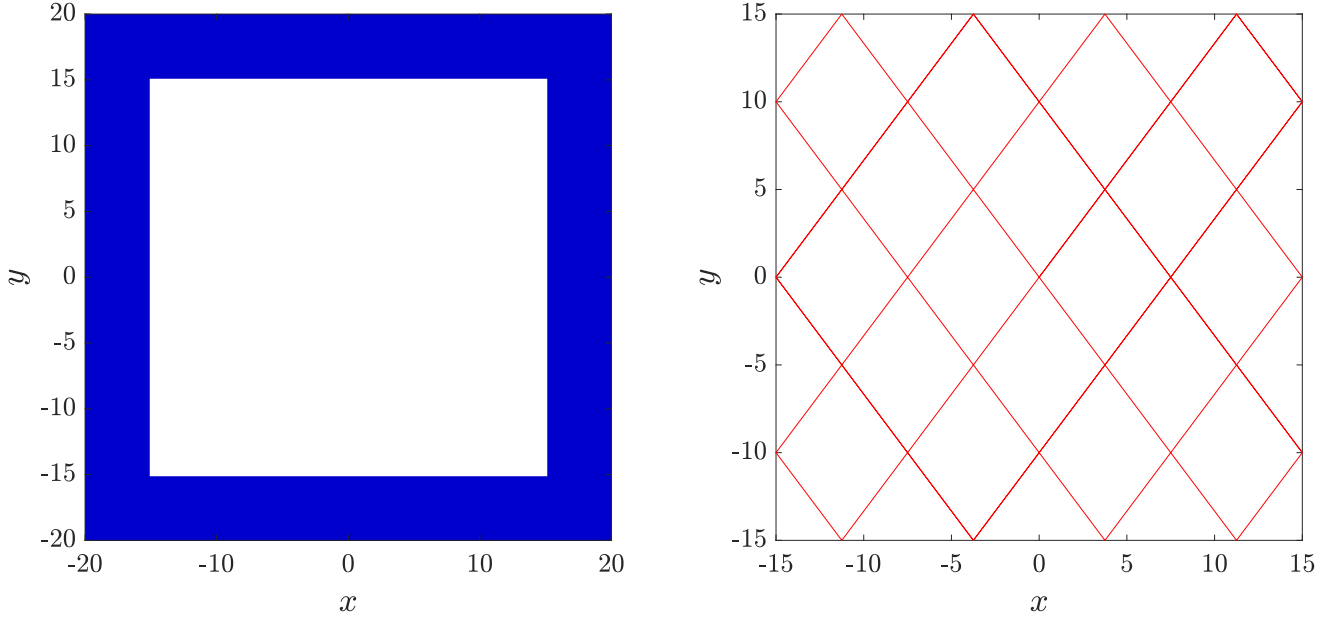
FIG. 2. (Left) Form of the square potential barrier given by (10). (Right) The trajectory of a classical *point* particle (right), in this potential.

This relative storage delay introduces a phase shift. Another way to describe the phase shift is as being due to the orbit actually travelling a small distance into the potential wall before being reflected. An incident orbit behaves as if it were laterally displaced upon reflection. This feature has been previously recognized as being analogous to the so-called Goos-Hänchen shift in optics, occurring also to solitary waves during their interaction with an interface; see, e.g., Ref. [33] and the discussion therein. We will discuss this in further quantitative detail in what follows below. It is interesting to note here that the Goos-Hänchen effect (GHE) has been recently encountered not only in the context of solitary waves interacting with external potentials but also of linear waves interacting with solitary ones [34].

C. Solitary wave square billiard with constant potential

We first consider a solitary wave placed in a billiard involving a square potential. It is known that classical square billiards are completely integrable [35]. Moreover, the orbits are periodic if $\tan\theta$ is rational, for the collision angle θ. When studying the evolution of solitary waves, we have firstly considered a square barrier potential of amplitude α, i.e.,

$$V(x,y) = \begin{cases} \alpha & \text{if } |x| > 3L/4 \text{ or } |y| > 3L/4 \\ 0 & \text{otherwise} \end{cases} \qquad (10)$$

The domain is taken with $L = 20$. This potential is shown on the left panel of Fig. 2.

In what follows, we have chosen $\cos\theta = 3/5$ for the initial collision angle. The right panel of Fig. 2, depicts the path of a classical point particle in this square potential. One can indeed see, in line with the theoretical expectation, that the dynamics is periodic for this choice of θ. On the other hand, in the left panel of Fig. 3, the path of the solitary wave with $v_0 = 0.02$ and $\alpha = 4$ is considered. One can see that in a way reminiscent of the classical billiard case, the dynamics is nearly periodic although the trajectories are different. The finite size of the solitary wave particle does not allow its center to reach the edge of the potential barrier (at $\pm 3L/4$ in each direction), but rather it effectively gets reflected "sooner". This is caused by the reflection rule of the trajectory of the solitary wave upon a constant potential (similar to what is observed in [32]). In other words, in line with our conceptual expectation based on the nature of the solitary wave, for such low speeds the solitary wave behaves as a particle interacting with a rectangular effective potential barrier (of smaller spatial extent).

Nevertheless, it is important to recognize that the solitary wave is not an infinitesimal particle mass. Instead, it features a finite width and for that reason this effective particle is reflected while its center of mass is still at a considerable distance from the domain boundary. There is some tunability of the width of the solitary wave (controlled by ω), however, the constraint of avoiding the cubic nonlinearity and associated collapse phenomenology does not allow for the freedom of (effectively) arbitrarily
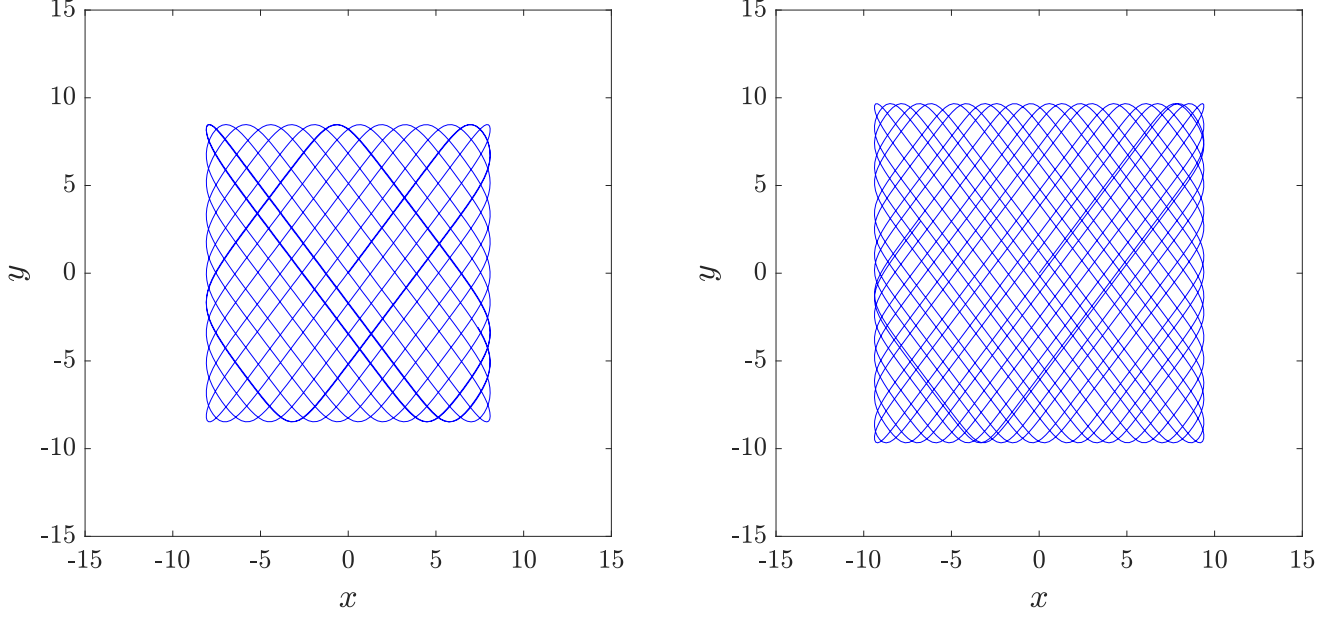
FIG. 3. Evolution of the center-of-mass of the finite-width solitary with $\alpha = 4$ and $v_0 = 0.02$, for $\omega = 0.5$ (left, a trajectory that effectively closes) and $\omega = 0.95$ (right, a trajectory that does not close). The final time of the simulation are $t = 4 \times 10^4$ and $t = 6 \times 10^4$, respectively. See also companion movies [37] and [38] depicting the evolution of the solitary wave dynamics.

selecting the solitonic width, as, e.g., can be done in one-dimensional such systems. Rather, here we are practically considering not only a soft potential (unless we examine the Dirichlet boundary condition case), but also a non-vanishing size particle that features a finite width and can, in principle, manifest internal modes capable of storing energy. This "deformability" of the solitary wave can also be detected in Fig. 3 at the positions of wall interactions where the trajectory of the solitary wave curves around in the reflection process, a manifestation of the GHE discussed above (see also details below).

As an interesting additional case example along this vein, in the right panel of Fig. 3, we have considered the example of the structure with the smallest width, namely $\omega = 0.95$. Interestingly, as we can see in that case the trajectory does not close, indicating the subtle nature of the corresponding phenomenology, for which as we highlighted, it is no longer the case that it purely depends on the angle of incidence, but also on other features of the soft particle, such as its width, its potential excitation of internal modes, etc. Hence, the closed orbit of the left panel of Fig. 3 should be considered to be a non-generic scenario for the deformable, solitary wave particles of interest herein. This can also be confirmed in the consideration of different settings (as that of the left panel of Fig. 3) but for different α (such as $\alpha = 10$) or different boundary conditions (such as Dirichlet). In both cases, shown in Fig. 4 left and right panels respectively, the trajectory can be seen not to close.

We have also explored how the above dynamics is altered when the velocity is increased and the barrier height is kept fixed; see, e.g., Fig. 5 for the solitary wave with $v_0 = 0.1$ and $\alpha = 4$. The resulting motion in this case as well is not periodic. If the wave moves more rapidly ($v_0 = 0.8$), it deforms nontrivially in the collisions with the barrier, and some radiation is emitted. The evolution of the coherent structure motion can be observed in more detail in the companion movies [37]–[44], where the square root of the density ($|\psi(x, y; t)|$) and its logarithm is tracked. One can see how the solitary wave approaches the barrier and spends some time in its vicinity before eventually being reflected. This process is central to our observation of the trajectories of the solitary waves (and their non-closed form), hence we focus on this further in what follows.

An explanation for the fact that the wave's center of mass does not reach the barrier is based on the intriguing observation of a *negative* Goos-Hänchen effect (see e.g. [36] for such an effect in one-dimensional optical systems, as well as [33] for a solitonic example). Figure 6 shows the evolution of the integrated norm with respect to x-coordinate, i.e. $|\phi_x(y, t)|^2 = \int \mathrm{d}x |\phi(x, y, t)|^2$ together with a scheme defining the Goos-Hänchen shift (GHs), Δ, for the collision of the solitary wave with a wall barrier of height α.

Notice that because of the GHs, the motion of the wave's center of mass when interacting with the wall can be approximated by a classical particle in a domain shrunk by a distance $\sigma = (\Delta \cot \theta)/2$. An important point is that in the square barrier, the impact angle of the solitary wave with the vertical lines of the square is the complementary to the angle of impact with the horizontal lines. Consequently, there will be two different GH shifts to account for, namely the one corresponding to an initial angle θ (denoted as Δ), and the one for $\theta_c = \pi/2 - \theta$ (denoted as θ_c, with the corresponding shrinkage $\sigma_c = (\Delta_c \tan \theta)/2$) in
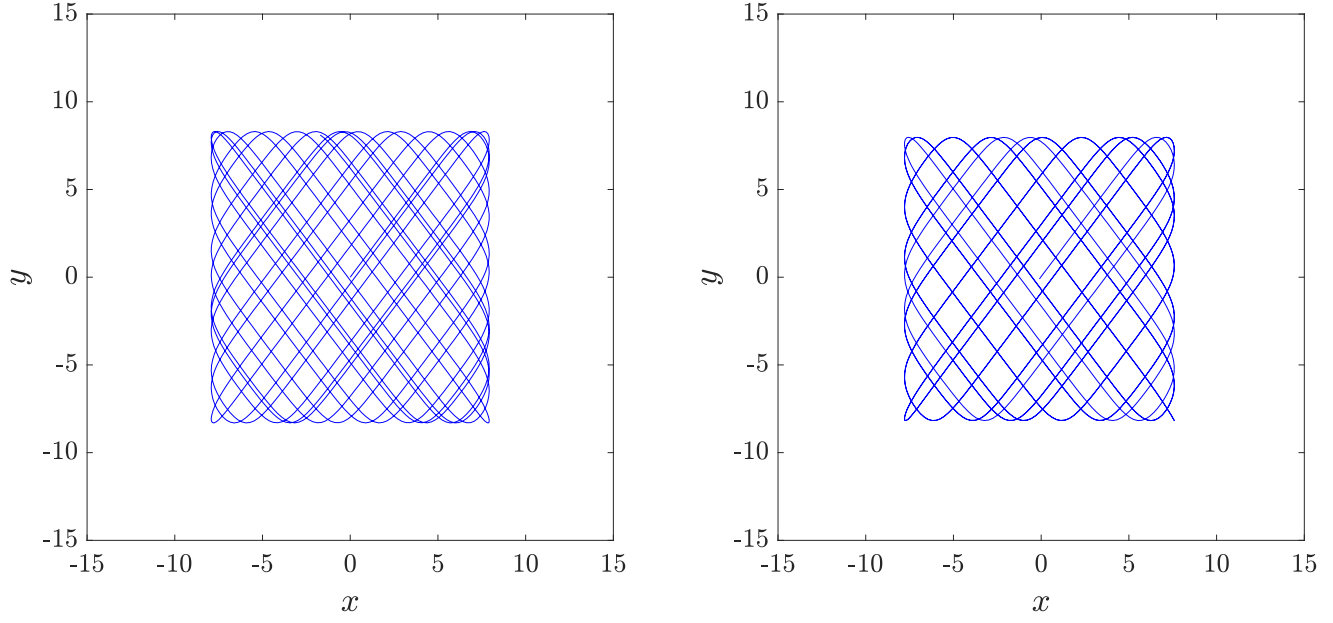
FIG. 4. Evolution of the center-of-mass of the solitary waves with $\alpha = 10$ (left panel) and Dirichlet boundary conditions (right panel), in the square barrier potential (10). In both cases, $v_0 = 0.02$ and $\omega = 0.5$. The final time of the simulation is $t = 4 \times 10^4$. See also companion movies [39] and [40] depicting the evolution of the solitary wave dynamics.
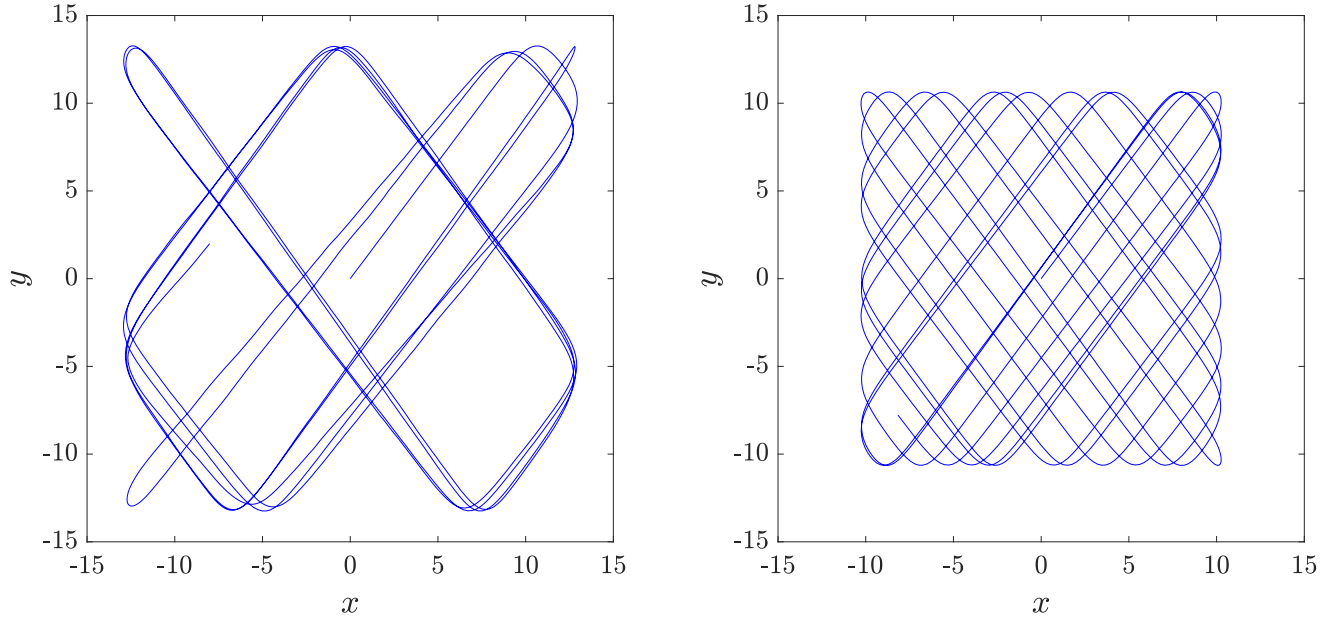

FIG. 5. Evolution of the center-of-mass of the solitary waves with $v_0 = 0.1$ (left panel) and $v_0 = 0.8$ (right panel), in the square barrier potential (10). In both cases, $\alpha = 4$ and $\omega = 0.5$. The final time of the simulation are $t = 8 \times 10^3$ and $t = 10^3$, respectively. See also companion movies [41] and [42] depicting the evolution of the solitary wave dynamics.
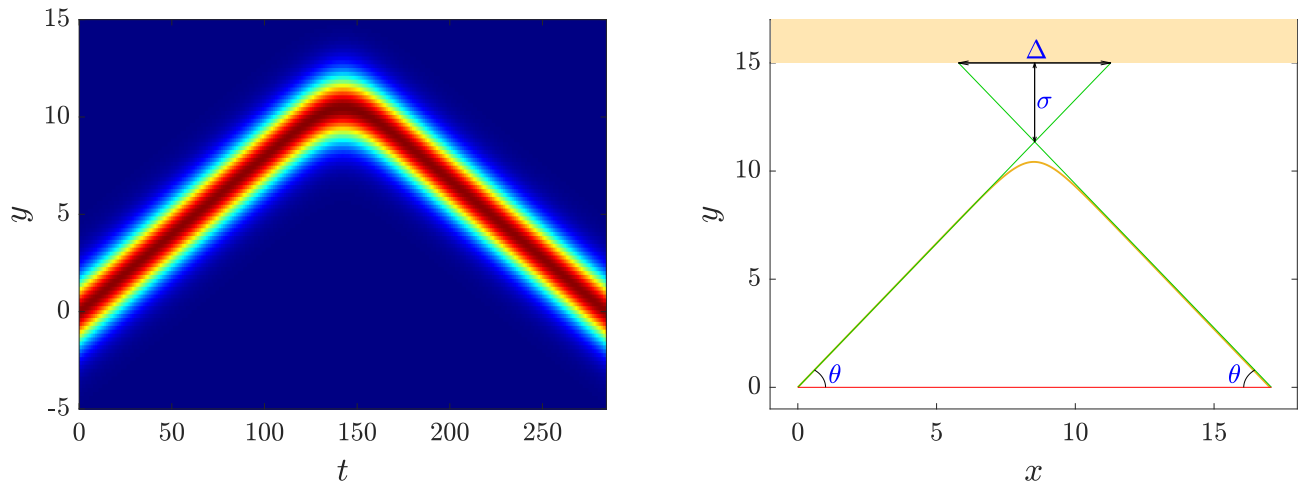
FIG. 6. (Left panel) Evolution of the projected solitary wave density when interacting with a wall barrier of height $\alpha = 4$; the initial velocity of the coherent structure is $v_0 = 0.1$ and the initial angle $\theta = \cos^{-1} 3/5$. (Right panel) Path followed by the center of mass of the wave together with a scheme indicating some relevant parameters like the Goos-Hänchen shift Δ or the domain shrinking σ.

the perpendicular direction. Then, the trajectory of the center of mass of the solitary wave can be approximated by a classical particle in a rectangle bounded by $|x| = 3L/4 - \sigma_c$ and $|y| = 3L/4 - \sigma$. Figure 7 shows the numerically computed dependence of the GHs with respect to v_0 for fixed $\omega = 0.5$, and also the dependence with ω for $v_0 = 0.1$. One can see that in the latter case, the minimum values of Δ and Δ_c are not attained for the narrowest solitary wave, i.e., that with $\omega = 0.95$, but rather around $\omega = 1.05$ (the particular value depends on the barrier height).

The above description based on the GHE enables a systematic understanding of the solitary wave interaction with a square billiard. Figure 8 shows the evolution of a classical particle in a shrunk domain by the GHs corresponding to a solitary wave in the presence of a barrier with $\alpha = 4$. This evolution is quantitatively compared with that of the center of mass of the coherent structure. Notice that until the second collision, the two trajectories overlap; the separation between them starts to subsequently appear because the wave interacts without following a perfectly straight line, but rather has a curved part in its trajectory. This weak effect compounds itself over time, eventually leading to the non-closure of the orbit. We have also checked that the relevant situation does not improve for larger α, or for Dirichlet boundary conditions. While this procedure allows for a highly accurate description of individual collisions, slight deviations from straight motion of our deformable effective particles ultimate lead to the non-closed trajectory, generic phenomenology observed herein.

D. Some other prototypical solitary wave billiards

We end this section by showing the outcome of the solitary wave dynamics in a Bunimovich stadium and a Sinai billiard (see the left top and bottom panels, respectively, of Fig. 9). Here, we are motivated by the chaotic nature of these billiards even for classical point particles and we seek to observe the dynamics of our deformable effective particle therein. In the first case, the barrier (composed by a square whose sides have a length 24 attached to two semicircles of radius 12) has a potential height of $\alpha = 4$ and is embedded into a domain $[-32, 32] \times [-16, 16]$, and the solitary wave is launched from $(0, 0)$. In the second case, the domain size is $[-24, 24] \times [-24, 24]$, encompassing a square barrier of side length 18 and a circular barrier of radius 2, both centered at $(0, 0)$, that have a potential height of $\alpha = 4$. Here, the solitary wave is launched from the point $(-8, -8)$. The path followed by the center of mass of the wave of initial velocity $v_0 = 0.02$ is depicted in the bottom panels of Fig. 9. In both cases, we can observe the chaotic nature of the dynamics which is reminiscent of the ergodic nature of the point particle case, yet again with a significant difference borne out of the GHE present in the solitonic case. The latter effect naturally, in this case as well, precludes the accessibility of a substantial region of the configuration space, similarly to the above presented square billiard case.

IV. CONCLUSIONS AND FUTURE CHALLENGES

In the present work, we have proposed a new paradigm for the dynamics of solitary waves, namely the study of solitonic billiards. We have judiciously selected a model that, on the one hand, is physically relevant, yet on the other hand avoids
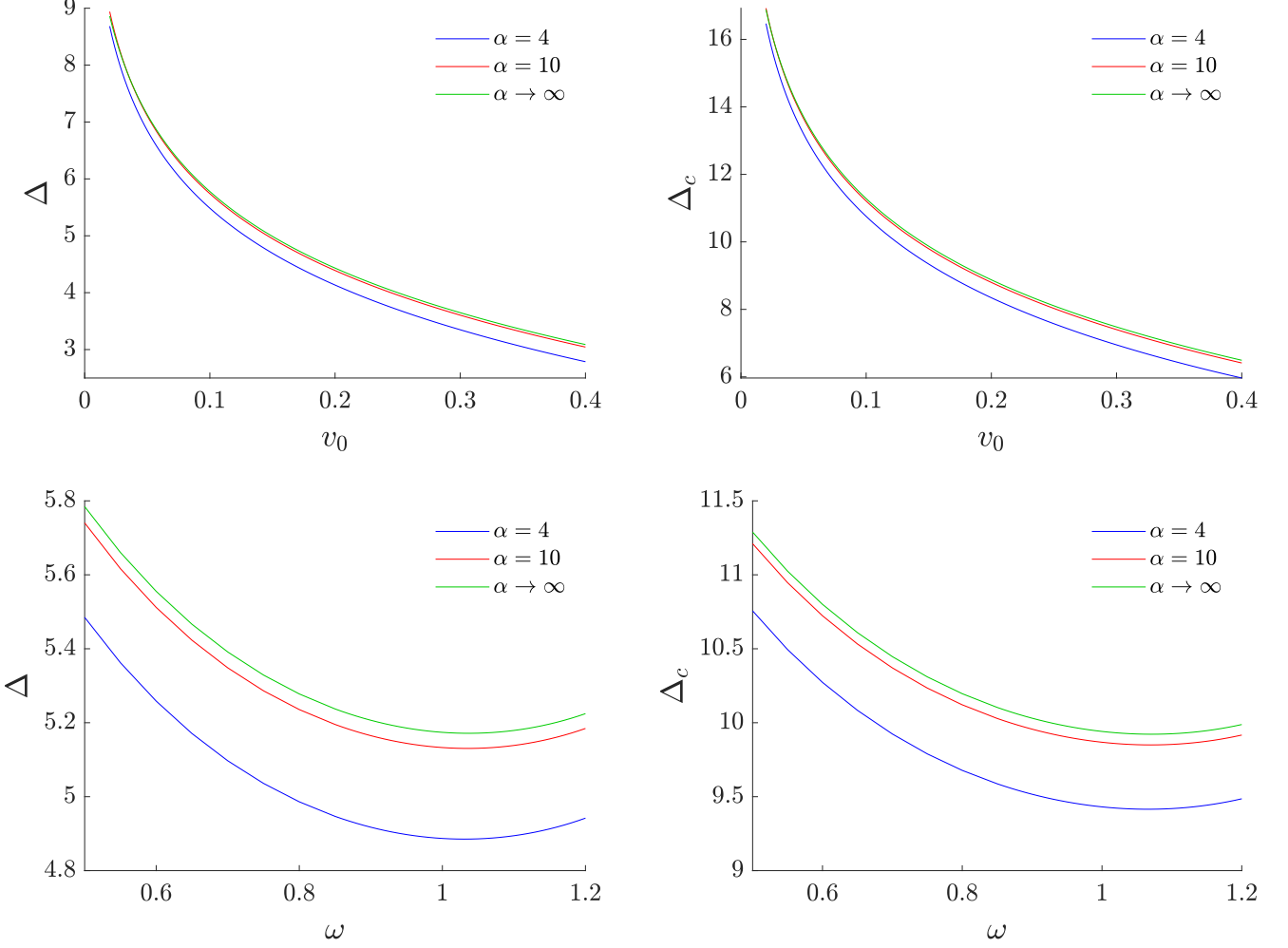
FIG. 7. Dependence of the Goos-Hänchen shift for $\theta = \cos^{-1}(3/5)$ (left panels) and $\theta = \cos^{-1}(4/5)$ (right panels) for fixed frequency $\omega = 0.5$ (top panels) and fixed initial speed $v_0 = 0.1$ (bottom panels). Dirichlet boundary conditions are denoted by $\alpha \to \infty$.

well-known pathologies of higher-dimensional NLS models, such as the presence of self-focusing and wave collapse [10]. By choosing the saturable nonlinearity model, we present a setting of relevance, e.g., to photorefractive optical crystals that possesses a Hamiltonian nature (in line with classical point-particle billiards), but which also has other key advantages, such as the ability to Galilean-boost the coherent structures. We believe that this is rendering the present paradigm a far-closer "wave billiard" example, to the point particle case, than, e.g., the dissipative example of [32]. We identified some important differences that this solitonic billiard features in comparison to the point particle case. Indeed, the finite width of the solitary particle and the non-integrable nature of the model present new possibilities including that of the collision storing some of the kinetic energy into internal mode oscillations, as well as that of the collision not being perfectly elastic. At the same time, we have observed the presence of a solitonic analogue of the (negative) Goos-Hänchen effect which also leads to significant deviations from the point particle case, including the effective shrinkage of the billiard domain. These features combined render even integrable point particle billiards non-integrable ones when considered in this solitonic realm (such as, e.g., the square/rectangular billiards). For completeness, we also examined the case of billiards such as the Bunimovich stadium or the Sinai billiard that are chaotic at the point-particle level and observed similar phenomenology (but with the above features still manifest) in the present setting.

We believe that this vein of studies is at a nascent stage and hence there are numerous opportunities for the future. It is interesting, for instance, to explore how the variation of the solitonic width (controlled by ω) would change the case considered herein. Furthermore, it would be of relevance to consider the Lyapunov exponents of the present wave billiard dynamics and to compare it with the corresponding quantities for the effective particle system, as a vein of quantitative comparison of the two systems, across different billiard settings. Such an understanding could lead to leverage the effective particle model towards analytical calculations in the future [45]. Another possibility would be to examine some case examples of models that are
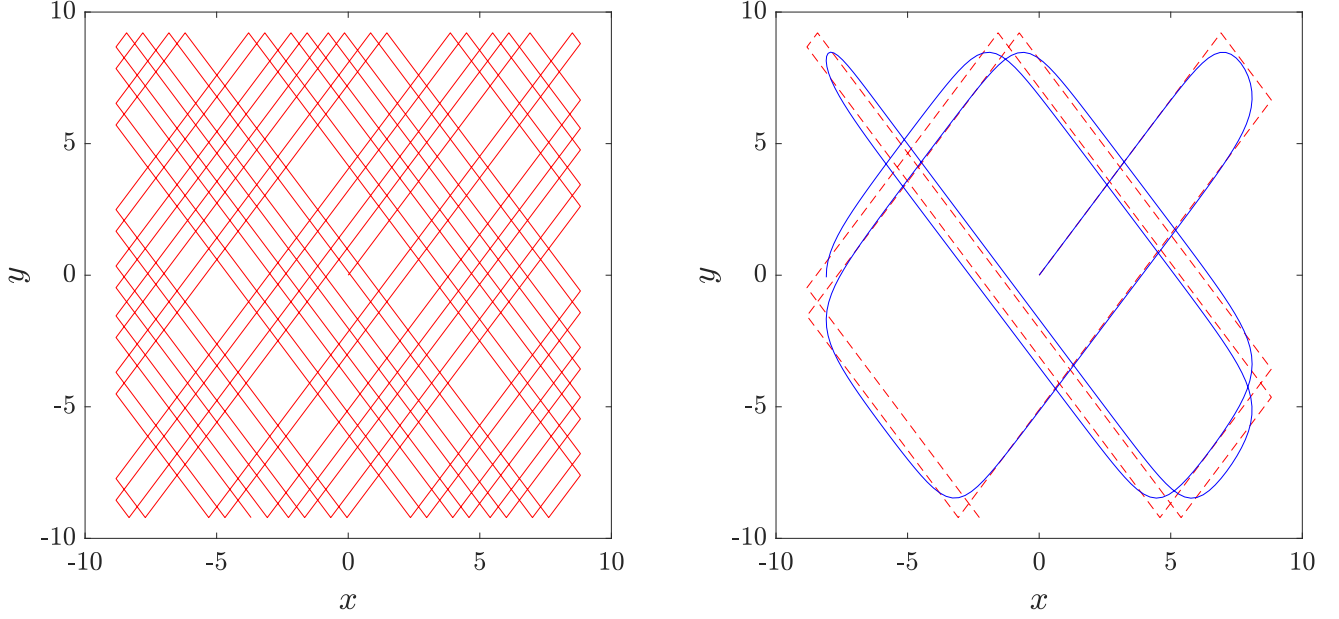
FIG. 8. Trajectory of a classical particle in a shrunk domain with a Goos-Hänchen shift corresponding to a solitary wave in a square barrier potential of height $\alpha = 4$. The left panel shows the evolution until $t = 4 \times 10^4$, whereas right panel captures the early stage up to $t = 8000$ and compares it with the evolution of the the center-of-mass of the solitary wave (full blue line). One can observe that up to the second collision with the barrier, the trajectories overlap, while at later times, they slightly deviate from each other. The remaining parameters are $v_0 = 0.02$ and $\omega = 0.5$.

integrable in the two-dimensional setting such as the Davey-Stewartson (or the Kadomtsev-Petviashvili) equation and explore how their integrable structures may fare in terms of similarities and differences to the non-integrable ones considered herein. It would also be of relevance to examine corresponding generalizations to higher dimensional settings and explore billiard enclosures and solitonic motion therein. These are only some of the possible directions emerging. Some of these are currently under consideration and will, hopefully, be reported upon in future publications.

[1] A. Hasegawa, *Solitons in Optical Communications*, Clarendon Press (Oxford, NY 1995).
[2] Yu.S. Kivshar and G.P. Agrawal, *Optical solitons: from fibers to photonic crystals*, Academic Press (San Diego, 2003).
[3] M. Kono and M. Škorić, *Nonlinear Physics of Plasmas*, Springer-Verlag (Heidelberg, 2010).
[4] C.J. Pethick and H. Smith, *Bose-Einstein condensation in dilute gases*, Cambridge University Press (Cambridge, 2002).
[5] L.P. Pitaevskii and S. Stringari, *Bose-Einstein Condensation*, Oxford University Press (Oxford, 2003).
[6] C. Kharif, E. Pelinovsky, and A. Slunyaev, *Rogue waves in the ocean*, Springer-Verlag (Berlin, 2009).
[7] M.J. Ablowitz and H. Segur, *Solitons and the Inverse Scattering Transform*, SIAM (Philadelphia, 1981).
[8] M.J. Ablowitz and P.A. Clarkson, *Solitons, Nonlinear Evolution Equations and Inverse Scattering*, Cambridge University Press (Cambridge, 1991).
[9] M.J. Ablowitz, B. Prinari, and A.D. Trubatch, *Discrete and Continuous Nonlinear Schrödinger Systems*, Cambridge University Press (Cambridge, 2004).
[10] C. Sulem and P.L. Sulem, *The Nonlinear Schrödinger Equation*, Springer-Verlag (New York, 1999).
[11] P.G. Kevrekidis, D.J. Frantzeskakis, and R. Carretero-González, *The Defocusing Nonlinear Schrödinger Equation*, SIAM (Philadelphia,
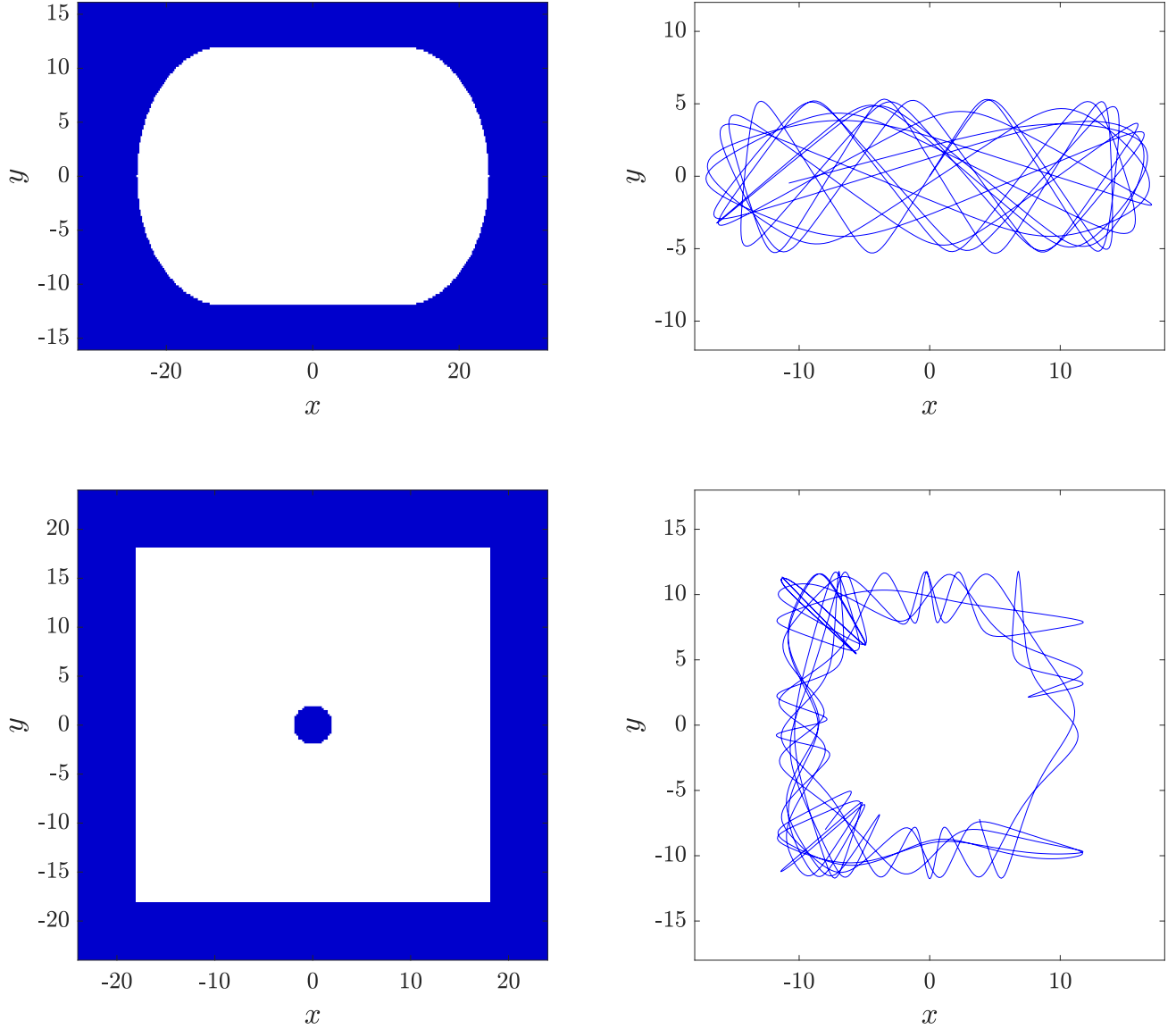
FIG. 9. Left panels: form of the Bunimovich stadium and Sinai billiard potentials. Right panels: evolution of the center-of-mass of the solitary wave with $v_0 = 0.02$ in a Bunimovich stadium (left panel) and a Sinai billiard (right panel). See also companion movies [43] and [44] depicting the evolution of the billiard dynamics.

 2015).
[12] Ya.G. Sinai, Russian Mathematical Surveys **25**, 137 (1970) .
[13] N. Chernov and R. Markarian, *Chaotic Billiards*, Mathematical survey and monographs **127**, American Mathematical Society (2006).
[14] See, e.g., https://mathworld.wolfram.com/Billiards.html
[15] L.A. Bunimovich, Commun. Math. Phys. **65**, 295 (1979).
[16] L.A. Bunimovich, Ya.G. Sinai, Commun. Math. Phys. **78**, 247 (1980).
[17] Ya.G. Sinai, Sov. Math Dokl. **4**, 1818 (1963).
[18] See, e.g., http://www.scholarpedia.org/article/Microwave_billiards_and_quantum_chaos
[19] A. Backer, Comput. Sci. Eng. **9**, 60 (2007).
[20] Č. Lozej, D. Lukman, M. Robnik, Phys. Rev. E **103**, 012204 (2021).
[21] Č. Lozej, G. Casati, T. Prosen, Phys. Rev. Research **4**, 013138 (2022).
[22] A. Kaplan, N. Friedman, M. Andersen, N. Davidson, Physica D **187**, 136 (2002).
[23] T. Kroetz, H.A. Oliveira, J.S.E. Portela, and R.L. Viana, Phys. Rev. E **94**, 022218 (2016)
[24] S. Gil-Gallegos, R. Klages, J. Solanpaa, and E. Rasanen, Eur. Phys. J. Special Topics **228**, 143 (2019).

[25] C. Zhang, J. Liu, M.G. Raizen, and Q. Niu Phys. Rev. Lett. **93**, 074101 (2004).

[26] L. Ermann, E. Vergini and D. L. Shepelyansky, EPL **111**, 50009 (2015).

[27] V. Milner, J. L. Hanssen, W. C. Campbell, and M. G. Raizen, Phys. Rev. Lett. **86**, 1514 (2001).

[28] J. Yang, New J. Phys. **6**, 47 (2004).

[29] Z.-H. Luo, W. Pang, B. Liu, Y. Li and B.A. Malomed, Frontiers of Physics **16**, 32201 (2021)

[30] Yu.S. Kivshar and G.P. Agrawal, *Optical solitons: from fibers to photonic crystals*, Academic Press (San Diego, 2003).

[31] K. Henderson, C. Ryu, C. MacCormick and M.G. Boshier, New J. Phys. **11** (2009) 043030.

[32] F. Prati, L.A. Lugiato, G. Tissoni and M. Brambilla. Phys. Rev. A **84**, 053852 (2011)

[33] J. Sánchez-Curto, P. Chamorro-Posada, J. Opt. **22**, 015502 (2020).

[34] V. Laliena, J. Campo, Adv. Electron. Mater. 2100782 (2021).

[35] https://en.wikipedia.org/wiki/Arithmetic_billiards

[36] M.C. Rechtsman, Y. Kartashov, F. Setzpfandt, H. Trompeter, L. Torner, T. Pertsch, U. Peschel, A. Szameit, Opt. Lett. **36**, 4446 (2011).

[37] The time evolution of the square root of the soliton density $|\psi(x, y; t)|$ (left panel) and its logarithm (right panel) is depicted in this and the following movies: https://www.dropbox.com/s/32a2oarpq4t2pdn/square_v02_alpha_4.gif

[38] https://www.dropbox.com/s/feenr73hwyr09q3/square_v02_alpha4_w95.gif

[39] https://www.dropbox.com/s/v7tzl1uaqqhfcde/square_v02_alpha_10.gif

[40] https://www.dropbox.com/s/6cmwb0ztdviz5aw/square_v02_dirichlet.gif

[41] https://www.dropbox.com/s/0xz0maglkdg6v2k/square_v1_alpha_4.gif

[42] https://www.dropbox.com/s/e69hsrnawbg1g85/square_v8_alpha_4.gif

[43] https://www.dropbox.com/s/paen31bardlqzrg/Bunimovich.gif

[44] https://www.dropbox.com/s/xjqk0qrvd4dfd9k/Sinai.gif

[45] As just one example of such calculations in a model involving successive reflections, see, e.g., V.A. Karyotis, C.A. Valagiannopoulos, IET Microw. Antennas Propag. **4**, 91 (2010).